The shape of things to come — Development and testing of a new marine vibrator source

Benoît Teyssandier[1] and John J. Sallas[2]

Abstract

Ten years ago, CGG launched a project to develop a new concept of marine vibrator (MV) technology. We present our work, concluding with the successful acquisition of a seismic image using an ocean-bottom-node 2D survey. The expectation for MV technology is that it could reduce ocean exposure to seismic source sound, enable new acquisition solutions, and improve seismic data quality. After consideration of our objectives in terms of imaging, productivity, acoustic efficiency, and operational risk, we developed two spectrally complementary prototypes to cover the seismic bandwidth. In practice, an array composed of several MV units is needed for images of comparable quality to those produced from air-gun data sets. Because coupling to the water is invariant, MV signals tend to be repeatable. Since far-field pressure is directly proportional to piston volumetric acceleration, the far-field radiation can be well controlled through accurate piston motion control. These features allow us to shape signals to match precisely a desired spectrum while observing equipment constraints. Over the last few years, an intensive validation process was conducted at our dedicated test facility. The MV units were exposed to 2000 hours of in-sea testing with only minor technical issues.

Introduction

Please do not be taken aback by our title: "The shape of things to come." We do not intend to predict a world such as that described in H. G. Wells' 1933 book of the same name. Our aim is to describe our work of updating an old technology — marine vibrator (MV) technology — to provide a versatile source option that can deliver a shaped spectral output capable of meeting our industry's future needs.

The successful introduction of marine air-gun technology by Bolt Associates in 1964 displaced other sources such as dynamite, gas gun, and sparker that were in widespread use earlier. (Stephen Chelminski received the SEG Virgil Kauffman Gold Medal in 1975 for his invention of the marine air gun.) Since that time, seismic marine sources have consisted primarily of arrays of several synchronized air guns that constructively deliver a sharp and highly energetic pulse (Caldwell and Dragoset, 2000). This impulsive source signature becomes the propagating wavelet, which enables subsurface illumination. Lack of source signature repeatability/controllability, the inability to produce ultra-low frequencies for image accuracy and resolution (Dellinger et al., 2016), and any possible impact on marine life (Hovem et al., 2012) are sufficient reasons to develop new technologies that are more effective in finding oil and gas deposits and/or tracking reservoir changes over time.

MV technology is a viable candidate to meet those needs. More than 15,000 miles of commercial seismic surveys were collected using hydraulic MVs prior to 1967 (Robinson, 1967). Over the years, there have been attempts to reintroduce MVs, but there was no major industry interest during the 1970s and 1980s (Broding et al., 1971; Baeten et al., 1988; Bouyoucos and Nelson, 1988). These attempts suffered from reliability problems and lack of low-frequency (LF) energy. The recent introduction of complementary and new technologies renewed interest in MV technology (Tenghamn, 2009; Jenkerson et al., 2013; Dellinger et al., 2016; Rassenfoss, 2016; Mougenot et al., 2017).

The MV is a versatile source that can emit a wide variety of signals such as a long tone with changing frequency (called a sweep) or a band-limited pseudorandom signal. For most situations, multiple MV units can be configured to operate as source arrays to increase the overall acoustic output. The MV provides capabilities of a controlled bandwidth and low radiated instantaneous acoustic pressure (the emitted energy is spread out over time) compared to an air-gun energy pulse, which has a peak amplitude and frequencies emitted beyond the desired seismic range. The additional benefit of providing a repeatable source signature is important for data quality and efficiency. The MV opens the door to continuous illumination techniques (Sallas, 2014; Hegna et al., 2018), gains in productivity thanks to simultaneous shooting, complementary illuminations, and field reconstruction techniques such as those numerically simulated by Laws et al. (2018).

First, we present our modeling effort leading to the predictability of source signature and validation testing of important features such as linearity and repeatability. Next, design considerations for tailored excitation signals, both pseudorandom signals and sweeps (swept sine wave signal, linear, or nonlinear), are discussed. Finally, we benchmark several techniques used to estimate the far-field radiation acquired during the 2D line ocean-bottom-node (OBN) survey and share the main results from our last sea trial — our first seismic image obtained using our MV source.

Marine vibrator principles and development

First conceived and developed by CGG in 2009, a small MV prototype was built to confirm our understanding of the ability of MVs to radiate efficiently at very low frequencies. After success with our first prototype, two full-size prototypes were built in 2012 followed by characterization, validation, and reliability tests. The full-size LF unit nominally operates at a depth of 15–35 m, while the high-frequency (HF) unit operates at 3–10 m depths. The LF and HF units are shown in Figure 1a and together form an optimized and efficient multiband system to cover the seismic

[1]CGG, Massy, France. E-mail: benoit.teyssandier@free.fr.
[2]GeoMagic, Plano, Texas, USA. E-mail: j.geomagic@gte.net.

Special Section: Acquisition and sensing
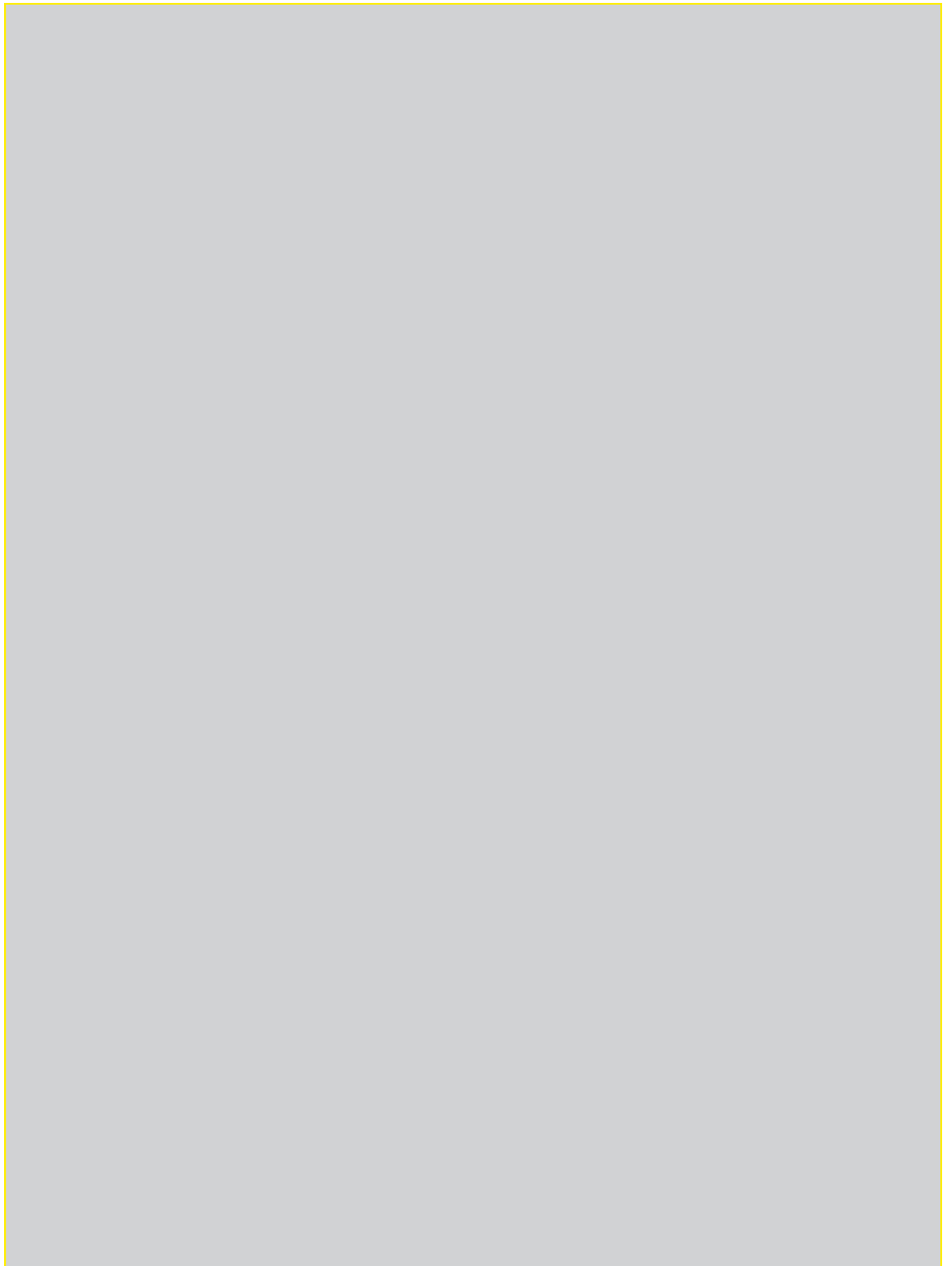
bandwidth. Each MV unit, also called twin transducers, includes two matched transducers mounted back to back to reduce the vibrations of the main body. The two pistons move synchronously in and out to create a volumetric acceleration of water and radiating P-waves. Ultimately, a far-field sound pressure is produced that is directly proportional to the source volumetric acceleration except for propagation delay and spherical spreading. Each transducer can be considered to act as a point source radiating equally in all directions, since the radiated wavelengths are greater than its physical dimensions. This transducer can be thought of as a closed-box projector system with a radiating piston driven by a rigidly attached high-efficiency linear motor. The sealed rear enclosure is pressurized using dry air through the use of an active hydrostatic balance system. In addition to the linear motors, each twin transducer is equipped with sensors for monitoring acceleration, displacement, temperature, current, and other variables. Each motor is driven by a pulse-width modulation amplifier. Additional embedded electronics for communication, signal conditioning, analog-to-digital conversion, and a high-speed digital controller for safety and motion feedback control (protection and linearization) are integrated inside the twin transducer enclosure. The hydrostatic balance system uses a controller to operate a pneumatic servo valve to automatically center the piston within a user-selectable range to maintain the full-stroke range needed for LF signal production.

A sea trial for seismic-imaging purposes along a 2D line took place in October 2017. Over a four-year prior period, we characterized and validated the subsystems making up a twin transducer. Figure 1b shows the key tests performed. They can be categorized as qualification and endurance tests for the linear motors using equivalent mass loading conditions and engineering validation tests under different operating conditions (workshop, pool, lake, and at sea). These trials helped us ruggedize our design. Much of our endurance testing took place in CGG's research and development sea test base in France, which has direct access to the ocean. After more than 1500 hours of testing for the LF twin transducer and 500 hours for the HF twin transducer, both units had only minor technical issues. Our tests included different excitation signals (tailored sweep signals, pseudorandom signals, and others).

Modeling

A special effort was made to develop useful models and simulation software that could be calibrated and validated. Electroacoustic projector systems are typically limited at low frequency and become highly nonlinear well before they reach their maximum acoustic output. Our model included the effects of nonlinear electrodynamic transduction. Considerable effort was given to modeling the pneumatic system and understanding the effect of pressure perturbations caused by swell. This is essential for performing realistic simulations. Our modeling efforts provided a full multiphysics modeling platform schematically shown in Figure 2. The modeling platform estimates performance for various source array geometries using the two different MV unit types (LF and HF). A pilot signal can then be computed for a sweep, pseudorandom sequence, or other choice, taking into account the constraints of the entire system
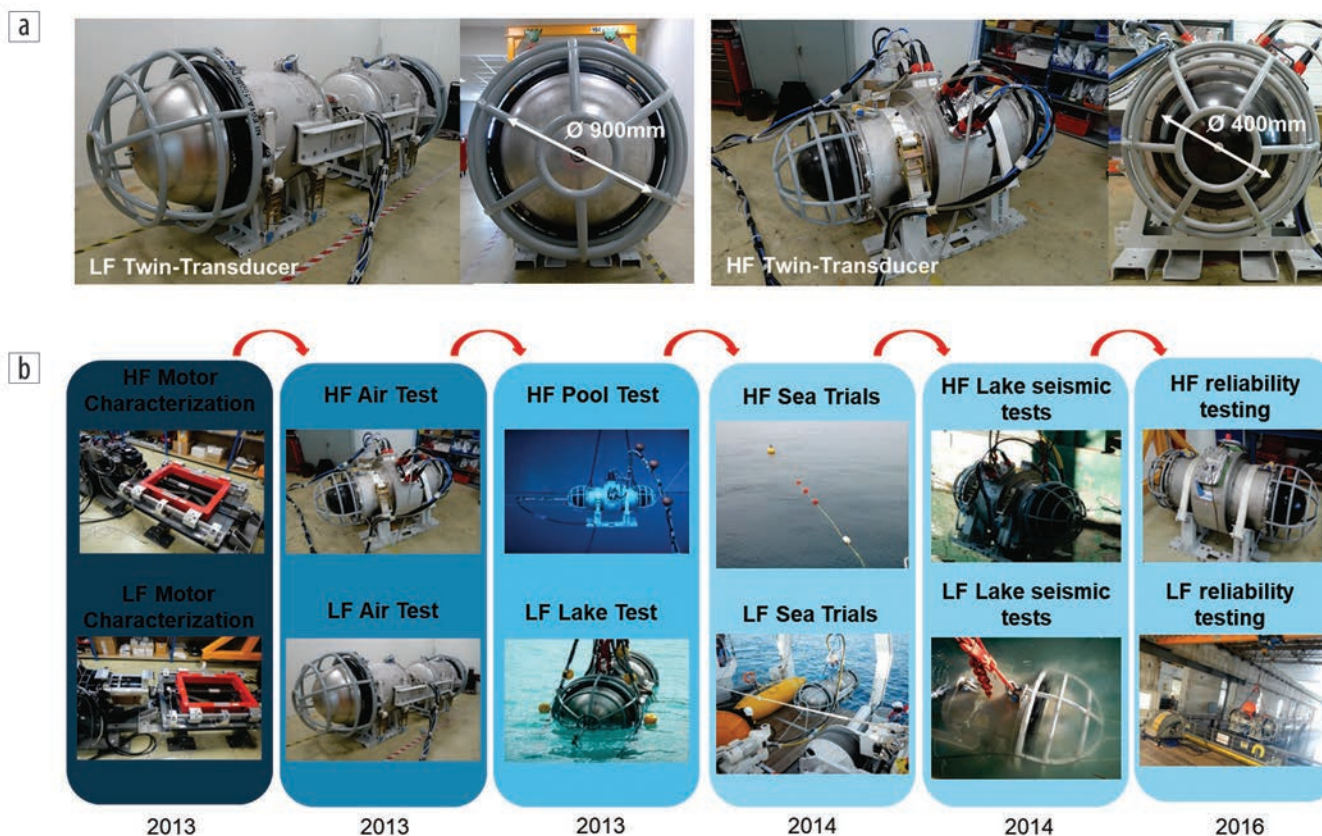

Figure 1. (a) CGG's MV elements (LF and HF), called twin transducers, with their respective piston diameters. (b) Validation and verification testing phase.

discussed later. Once the pilot is computed, the far-field signature can be computed for any point in a half-space domain, representing a semiinfinite layer of water below the sea surface. The user can select from different kinds of directivity plotting formats. Finally, some key performance indicators are computed, and an automatic performance report can be generated. One important consideration is the effect of mutual coupling between elements (Rossi, 1988; Sherman and Butler, 2008), which can have significant impact on the configuration of an MV source array as seen in the next section.

Accurate modeling of the source signature is important for sweep design, array design, and imaging. Acoustic modeling is useful for addressing two important concerns: the radiation impedance of the source and accurate estimation of the source signature. The

Figure 2. CGG's MV source modeling principle for computation of both real-time and frequency-domain performance.

term radiation impedance is the reactive force of the water acting on the piston face divided by the acoustic piston's axial velocity for a given frequency. Radiation impedance is a frequency-dependent complex number with a real part called radiation resistance and an imaginary part called radiation reactance. For pistons with dimensions less than one-half wavelength, the radiation reactance is much greater than the radiation resistance. From an engineering standpoint, the radiation reactance can be modeled as a mass loading on the piston called a radiation mass.

Typically, the term radiation impedance is used in the context of a single acoustic piston acting in free field (what we will refer to as self-impedance). For us, things are more complicated, and we have to consider the loading effect of the free-surface reflection and contributions of other MVs in our array on the acoustic piston of interest. We introduce the term total source radiation impedance. Two components make up the total source radiation impedance: self-impedance and mutual impedance. Self-impedance describes the load on a single acoustic piston acting alone when operating in a free field. Mutual impedance can be split into two parts: (1) the load contribution due to direct arrivals from other elements of the source array and (2) pressure waves due to reflected energy from all source elements. In some array designs, loading from other source elements can exceed 30% of the total source radiation impedance. The mutual coupling between array elements is a key factor in our acoustic modeling, since poor choices can lead to performance degradation. For us, the total radiation impedance is greater than the driven structural mass and contributes to more than 70% of the total actuator load. The radiation impedance model helps predict the load the linear actuator has to drive and any accompanying constraints. Knowledge of the constraints helps later with the design of efficient sweep signals.

Finite-element analysis was used to determine the expected total loading and structural rigidity for candidate designs. Recall,
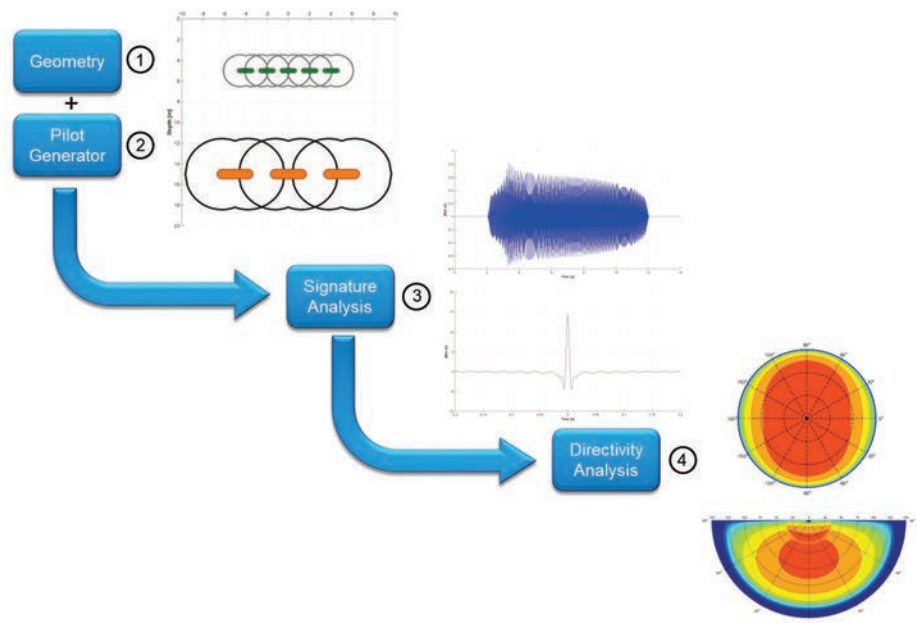
self-impedance varies with frequency and consists of a real and an imaginary part. The real part represents the radiated energy, while the imaginary part represents a reactive load that for small radiators can be thought of as a mass loading (radiation mass). The radiation mass is a function of piston diameter (increasing as the cube of the diameter) and profile shape, where a flat piston has a significantly greater radiation mass than a piston with an elongated conical profile, but there are other considerations. The designer must also take into account the structural mass when looking at the total load to be driven, the operating bandwidth, linear motor specifications, and static forces due to operating depth. We chose a hemispherical piston shape in both our LF and HF vibrators, since it offered the best trade-off in terms of structural rigidity, structural mass, ease of construction, and reduced self-impedance. In our current design, the LF piston has a 900 mm diameter, while our HF piston is 400 mm in diameter. Our LF vibrator piston is a stainless-steel weldment with a reinforced rubber seal, while the HF vibrator piston is made from a carbon-fiber composite with an integral carbon-fiber seal.

Mutual impedance describes that portion of the total source radiation impedance that is due to interaction with other acoustic projectors and/or operating environment. This interaction is due to pressure waves impinging on the piston due to direct arrivals from other sources and from reflected P-wave contributions from both the projector of interest and different projectors. The resultant interaction force can be considerable. For our back-to-back design, the two pistons are not widely spaced. The mutual impedance is important as we plan to operate using subarrays to boost output, so other array elements may operate in close proximity to one another because we want the subarray to look like a point source. One way to investigate mutual-impedance effects and validate our model is to perform pool testing, where the walls of the pool have positive reflection coefficients, and those reflections mimic the effect of having
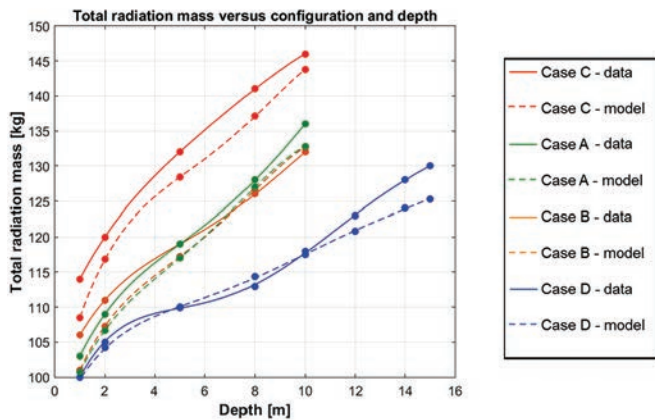
Figure 3. Total radiation mass versus water depth for several configurations.

Table 1. Different case study used for the experimental mutual coupling analysis.

Config.	Naming
	Case A: Back to Back @ 3 m
	Case B: Side by side @ 3 m
	Case C: Face to Face @ 1 m
	Case D: Single

other projectors operating nearby. In addition, the pool surface with its negative reflection coefficient is similar to the ocean's free-surface, and mutual-impedance effects due to surface reflections can be included. In reality, things are more complex due to multiple reflections leading to a "hall of mirrors" effect from walls in particular. Our first test to validate our models for source radiation impedance took place at the French Research Institute for Exploitation of the Sea's pool test site in 2011 using our first LF prototype with a 760 mm diameter hemispherical piston. Our measured comparison between data and model appears in Figure 3. Those tests were conducted in a pool that was 20 m deep with 15 m wide flat vertical walls on three sides. A fourth vertical wall's bottom half was vertical, and the upper half opened into a larger shallow pool. The twin piston design was split so the two halves could be arranged in different ways to facilitate these tests, with several configurations given in Table 1 using different depths. Figure 3 gives two main trends. (1) We see that the model and the measurements are in good agreement. Greater differences can be seen in the face-to-face 1 m situation, where the transducers are getting so close to each other that the model reaches its limits. (2) As mentioned earlier, getting close to the surface reduces the total radiation mass (self and mutual impedances), whereas a clear increase in the total radiation mass can be achieved by putting transducers close together operating in phase. The closer they are, the greater the total radiation mass.

Typical excitation signals used and their characteristics

Excitation signal design tools for both sweeps and pseudorandom signals have been developed for use with MV technology. For engineering purposes, sweeps (swept sine wave signals) can be considered to emit only one frequency at a time with one-to-one mapping between frequency and time. Sweeps include linear sweeps and nonlinear sweeps. By contrast, pseudorandom signals can be designed to emit a wide range of frequencies simultaneously throughout their sweep length. We have adapted techniques used for land vibrators to emit a desired energy spectrum while maximizing the output energy without exceeding equipment and operating limits. Application of these techniques helps increase data acquisition productivity. The approach is different for swept sine wave versus pseudorandom signals.

Our MV units have the following equipment limitations: stroke, current, voltage, velocity, and dissipated power. These constraints are shown for both twin transducers in Figures 4a and 4b. The gray area shows the nominal operating region. The limits defining the maximum amplitudes that the two elements are able to reach safely are shown in Figure 4c. For low frequencies below resonance, we are limited by current and/or stroke (displacement). Our electric actuator has a displacement range over which the motor behaves linearly, and beyond that there are mechanical stops. For frequencies far below resonance, we are current limited due to the high force required to overcome trapped air volume spring and suspension stiffness, because we hit this limit before we are stroke limited. For low frequencies just below resonance, we are no longer current limited but stroke limited. At or near resonance, we can be velocity and/or voltage limited and/or power limited. Typically, the velocity limit is set at 2 m/s to accommodate linear-bearing guidelines. Above resonance and at higher frequencies, the issue is typically power or current limit. At very high frequencies, both current and voltage can limit output. An acceleration constraint based on operating depth to avoid water cavitation is an option.

For swept sine waves, the sweep design follows a procedure similar to that used for land vibrators and described in Sallas (2010). Instead of ground force, piston acceleration is what we need to control, since it represents the fluid volumetric acceleration and is directly related to the P-wave signal. To compensate for equipment constraints that do not allow the generation of high output signals, we utilize nonlinear sweeps. The dwell time at a particular frequency is increased to reach the target energy required for that frequency. For example, a low-dwell sweep may be used to build up LF energy to compensate for a piston stroke limitation. Dwell is the reciprocal of the time derivative of frequency (seconds/Hertz).

For our pseudorandom signals, we have different frequencies emitted simultaneously as shown in Figure 5. Methods that rely

on sinusoidal steady-state solutions are not applicable, and a time-domain solution is required. In this case, a candidate pseudorandom signal is spectrally shaped to comply with a desired piston-acceleration target spectrum. The candidate signal is adjusted iteratively until the target spectrum is achieved without exceeding any equipment limits. Our procedure has an option for performing joint optimization, where it may be desirable to create pseudorandom signals for multiple sources operating simultaneously that have spectral overlap or to mitigate residual shot noise.

Repeatability and linearity

While endurance testing at our sea test base facilities in 2016, we were able to implement data quality-control (QC) management routinely. Repeatability and linearity performance are discussed next based on data acquired with the LF twin transducer. A set of 200 linear sweeps starting at 5 Hz and ending at 25 Hz over a sweep length of 20 s will be considered.

Repeatability. MV repeatability is a key differentiator with air-gun technology. Poor repeatability can result in illumination instability. For land vibrators, repeatability can be problematic due to variable earth coupling. For MVs with linear motors, the device is inherently more linear, and coupling with the water is very repeatable. By having access to the pilot (reference signal) and the piston axial accelerometer signal, a tracking transfer function can be updated continuously. Figure 6 shows magnitude and phase performance. Because the tracking was so good, we provided a zoom on both magnitude and phase above 20 Hz. Excellent repeatability can be seen in this example. For both representations, the average response and its standard deviation are plotted. Over the sweep bandwidth, the tracking in amplitude is close to 0 dB, and a zero-phase response was achieved with the help from precompensation.

Linearity. A key aspect of an acoustic/seismic source is its ability to faithfully output a signal that is linearly related to its input. Nonlinear behavior leads to harmonic distortion that can introduce unwanted artifacts in correlated data. Despite improved
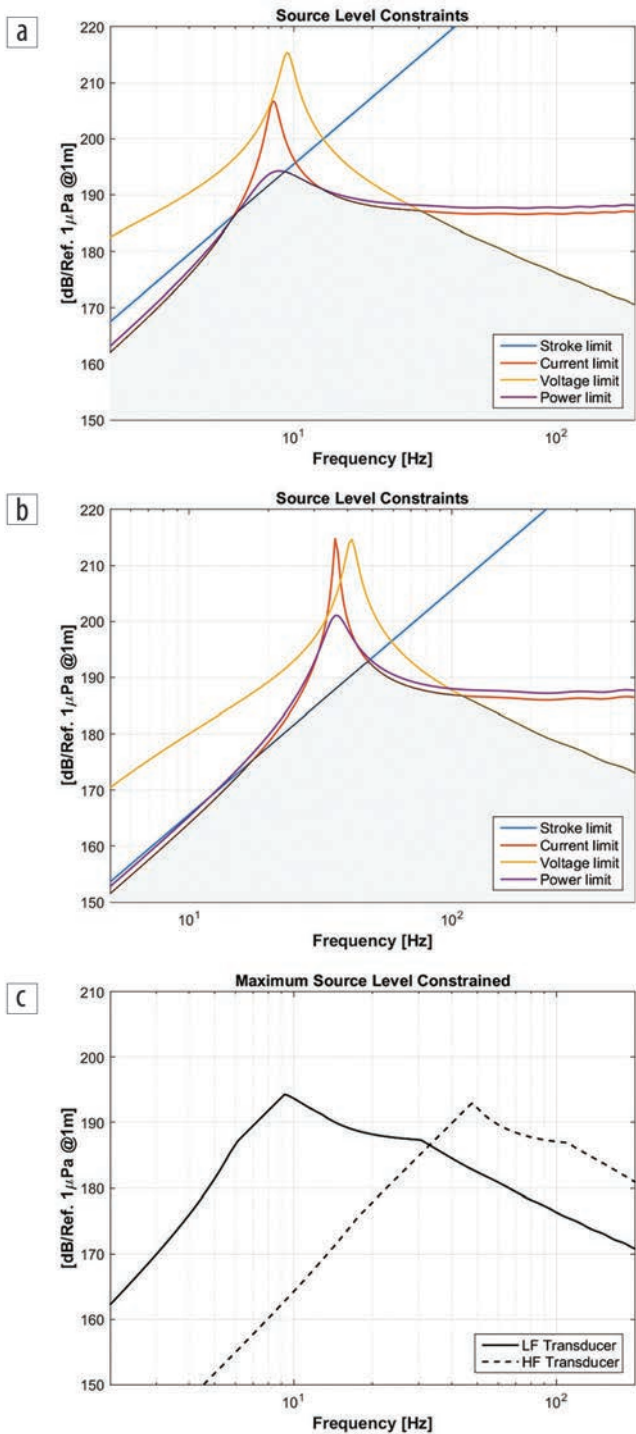
Figure 4. Constraints and limitations on source level produced by both transducer types. (a) LF transducer constraints and domain of validity. (b) HF transducer constraints and domain of validity. (c) Constrained levels for LF and HF transducers.
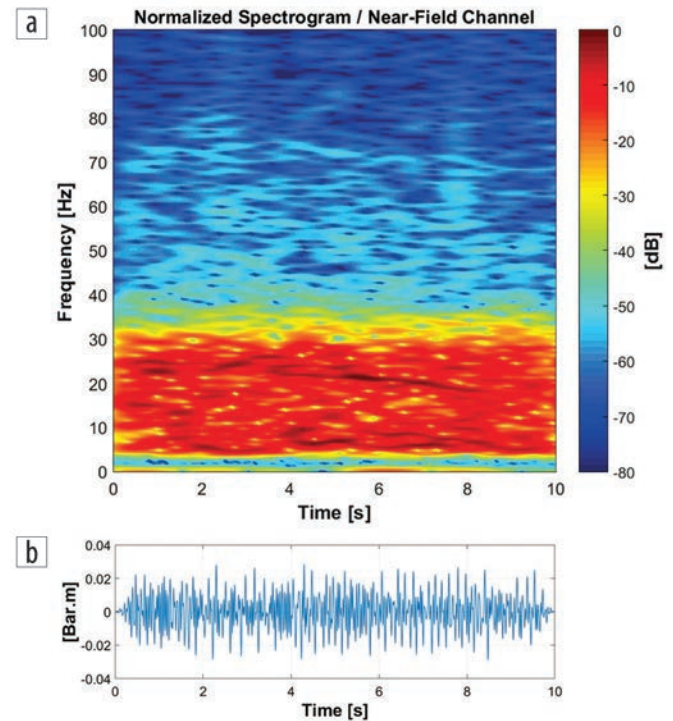
Figure 5. (a) Spectrogram of a pseudorandom signal over 10 s and showing a full-power bandwidth from 5 to 25 Hz with a 3 Hz spectral taper on both ends. (b) Pseudorandom signal waveform shown in the time domain and observed at an NFH.

control algorithms, land vibrator distortion still remains an issue since it can introduce crosstalk when simultaneous sweep techniques are used. Crosstalk can lead to considerable efforts in processing to mitigate its effect. Early on, we were successful in minimizing MV nonlinearities typically introduced by the linear motor whose force is dependent on the armature position, coil current, and magnet temperature. Suspension systems can also introduce nonlinear behavior for large piston displacement. Due to the high-performance linear motor in our MV twin transducers, the total harmonic distortion (THD) measured is less than 3.5% or –30 dB over their nominal seismic bandwidths as seen in Figure 7. Using

the previous data set, the spectral THD was computed for 200 linear sweeps from 5 to 25 Hz and over 20 s and displayed on a percent scale in Figure 7b. The mean value and standard deviation are also plotted. Over the specified bandwidth, the THD was less than 3.5% showing good MV fidelity and linearity. Figure 7a shows a spectrogram (time-frequency representation) of a sweep chosen randomly from the 200 sweeps used for this investigation. The linear instantaneous frequency law of the fundamental component can be clearly seen with several upper harmonic components. The color decibel contour display was used so that the low level of harmonic content can be easily observed.
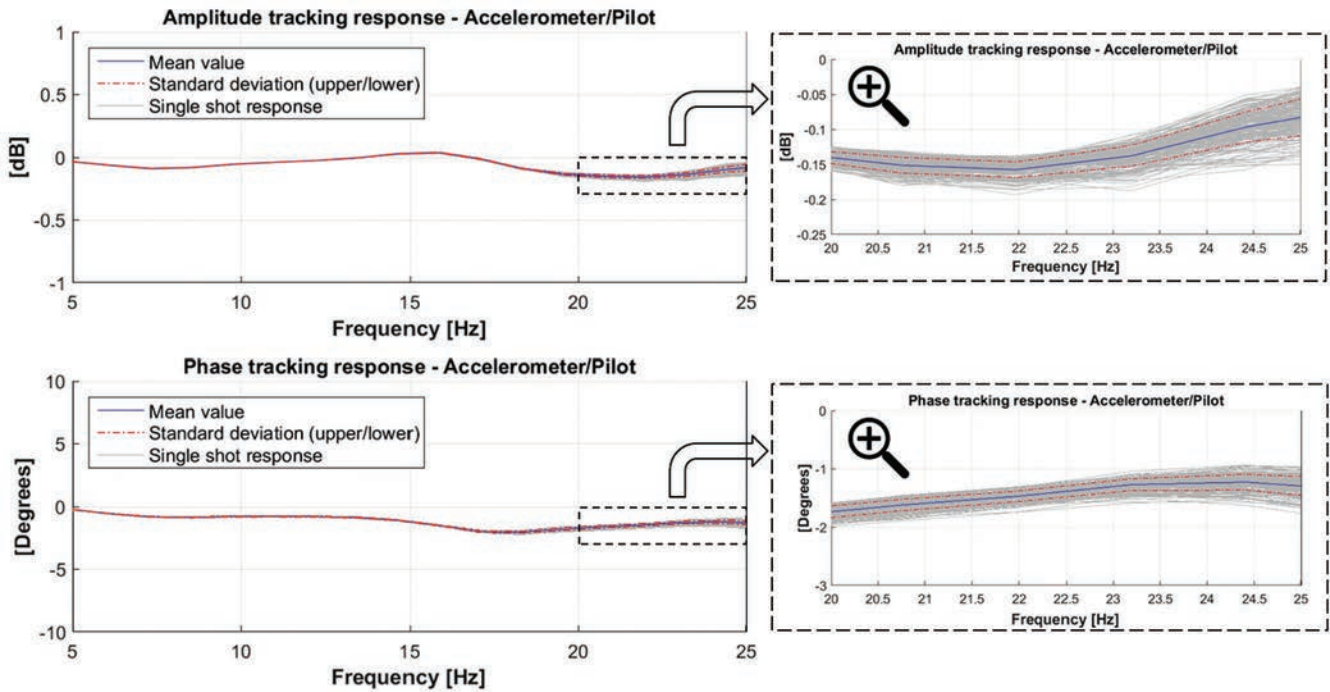

Figure 6. Transfer functions computed over a sequence of 200 sweeps in a row (linear sweep over 20 s from 5 to 25 Hz) showing a high degree of repeatability. Data acquired in our sea test base facilities.
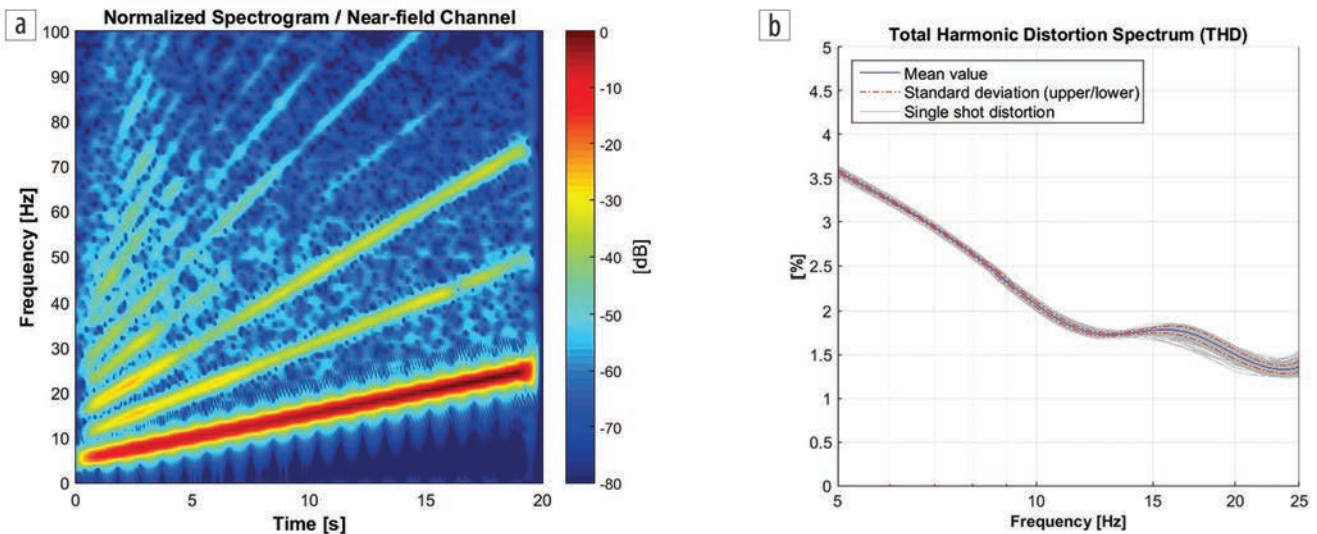

Figure 7. NFH measurements. (a) Spectrogram of a single sweep (linear sweep over 20 s from 5 to 25 Hz). (b) THD spectrum over a sequence of 200 sweeps in a row showing a very low standard deviation and extremely low distortion over the entire frequency bandwidth.

Sweeps versus pseudorandom signals

As part of our MV project, we developed software tools for designing pseudorandom signals with special properties and spectral shapes that would not exceed equipment limits. Pseudorandom signals generally have less energy than swept sine waves with the same temporal peak values; however, depending upon the nature of equipment constraints and signal bandwidth, this is not always the case. Generation of low frequency requires high piston displacement, where we may be stroke limited. A high-energy flat target spectrum may not be possible to achieve using a linear sweep because the required high piston acceleration cannot be generated at the low frequency. We can compensate by using a low-dwell sweep, but this may require a long dwell time at low frequencies to build up the LF energy. A special pseudorandom signal can be used instead. By using means similar to level compression, the pseudorandom signal can be boosted with both low and other frequencies simultaneously produced. Another way to think about this is that the wave shape of the pseudorandom signal that contains low frequencies and high frequencies can be tailored so that in some instances HF components emitted at the same time can help keep the piston away from its stops.

When pseudorandom signals are applied to nonlinear systems, intermodulation distortion (IMD) is produced. With pseudorandom signals, we have a superposition of multiple frequencies, but due to the nonlinearity, we get a mixing effect that produces not only harmonics of the input signal but also sum and difference spectral components. After correlation, IMD artifacts are smeared in frequency time and are more difficult to remove in processing than harmonic distortion produced using a swept sine wave excitation signal. IMD has not been an issue with our MV units due to their excellent linear performance. This enables us to generate pseudorandom signals with high fidelity.

Pseudorandom signals can be created using the joint-optimization procedure method mentioned earlier to create suites of signals that are only weakly correlated over a time interval of interest. A given source can be programmed to rotate through a set of pseudorandom signals as shot locations change. The rotation schedule can be coordinated with schedules used by other sources operating simultaneously to reduce crosstalk. This is a useful alternative to methods like phase encoding that have found use in swept sine wave signals to reduce crosstalk due to residual shot noise or other sources. Where we may have several different crews operating in the same region, pseudorandom signals could help reduce interference between adjacent MV crews.

Seismic imaging/sea trials 2017

An OBN 2D line survey was performed in the North Sea off the west coast of Bergen, Norway. The receiver line used 200 seismic nodes at 50 m spacing. Several acquisition lines were acquired with our MV prototypes using different bandwidths, different types of signals (mainly sweeps and pseudorandom signals), and different acquisition techniques (with and without listening time, phase coding sequence, and others). To objectively benchmark our MV units, a small air-gun source (a single subarray) with a selectable volume (170, 290, 340, and 500 in³) was used to acquire the same 2D line several times. Two main results follow: a vertical far-field signature spectrum estimate using three different but complementary monitoring techniques and our first processed seismic image from our OBN line using our MV technology.

Vertical far-field radiation estimates. Since we only had one LF and one HF unit, we elected to cover the seismic band of interest by taking several line passes, each covering different subbands. Our LF unit at 24 m depth covered the bands [3 Hz, 6 Hz] in 40 s and [5 Hz, 25 Hz] 12 s. The HF unit covered [20 Hz, 40 Hz] in 20 s at 11 m depth and [40 Hz, 75 Hz] 8 s at 7.4 m depth.

We found that estimating the radiated vertical far-field spectral signature was a useful tool for QC. The spectra for the four bandwidths were estimated using three different methods. First, direct extraction of the vertical far-field signature from the OBN data was performed using their hydrophone channels. Second, an indirect method that used the sum of the piston accelerations to estimate the total volumetric acceleration of an equivalent monopole was used, since both pistons are very close to one another (2 m apart for LF and 1 m apart for HF) and operate synchronously. As we do for air guns, knowing the depth and surface reflectivity, we can use notional sources to include the effect of the surface ghost. For MV arrays, by measuring all the piston accelerations, we can use superposition to estimate the resultant wavefield. Because MVs are well controlled and synchronized in phase to within a couple of degrees of one another, source signature estimates for MV arrays can be quite accurate. The third method was also an indirect method based on the near-field hydrophone (NFH) technique, as we do for air guns. NFH data can provide an independent measurement/validation of source performance and supplement information derived from piston-acceleration measurements.

Energy spectral densities (ESD) shown in Figure 8 were obtained using the following procedure. For the MV source, 10 sweeps per bandwidth were selected randomly along the acquisition line. Note bandwidth is abbreviated as BW in Figure 8. Similarly, 10 randomly selected shots from the 290 in³ air-gun (Sercel G-Source II air gun, 2000 psi, operating at 7 m depth) line were used. For the MV source, the vertical far-field signatures along with their spectral densities were computed using the three methods described earlier. Figures 8b–8d show the average ESD for each bandwidth for the 10 selected sweeps. The time window and bandpass filter operators were used in the MV OBN data-extraction process, introducing minor ripple artifacts in evidence on either side of the spectral bands in Figure 8d. For the 290 in³ air-gun source, only the OBN extraction technique was used. Figure 8e shows the average ESD for the 10 selected shots. All averaged spectral densities are labeled with their respective modeling (black dashed lines) with a good match between modeled and measured results.

Seismic imaging. The CGG seismic processing group produced the seismic image shown in Figure 9a acquired with our MV sources. The MV image is comparable to the one produced by a 290 in³ array source shown in Figure 9b and band limited to 75 Hz.
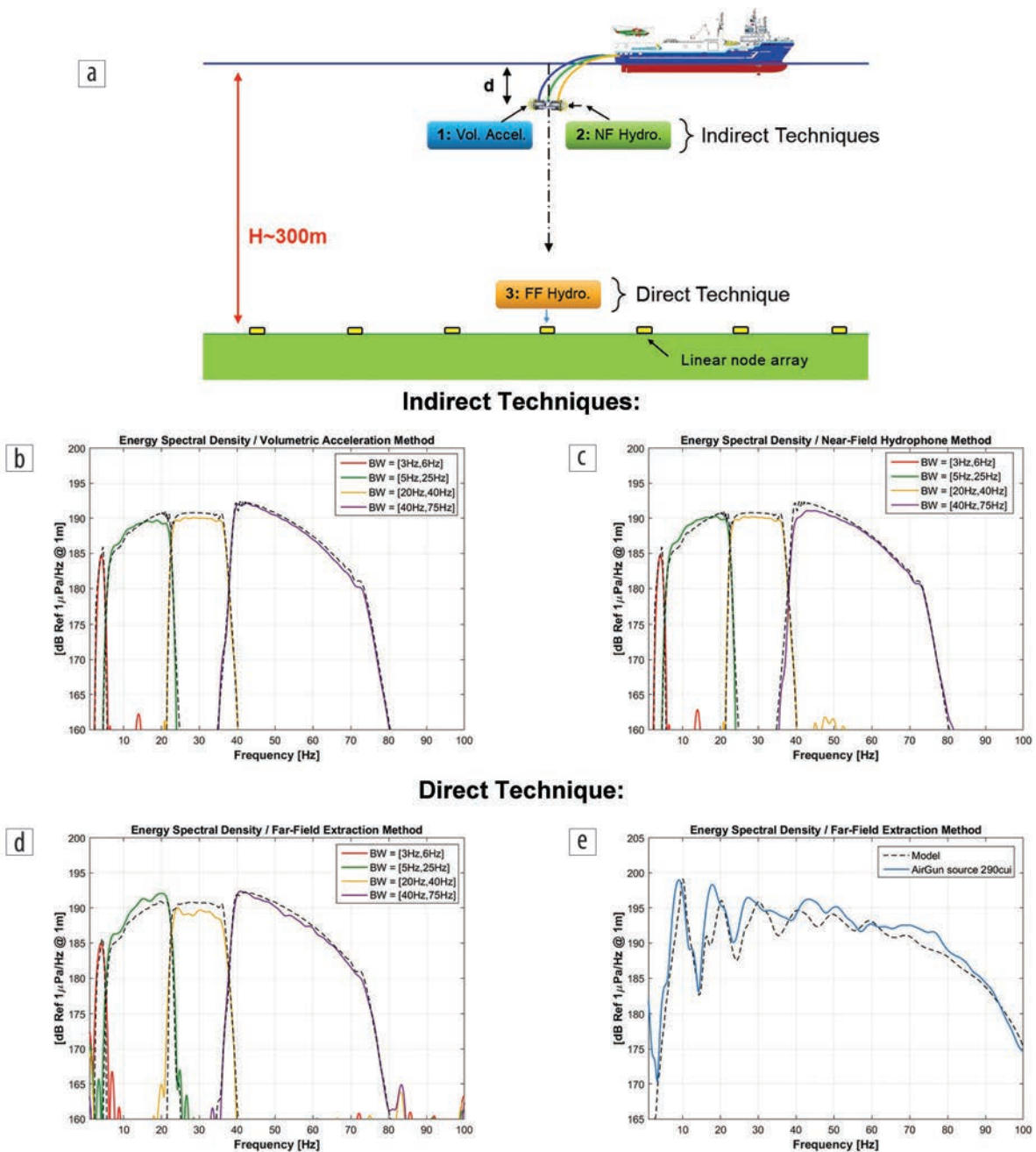
Figure 8. Averaged spectral densities over 10 shots/sweeps along the vertical direction. Modeling given by black dashed lines. (a) Schematic showing the direct and indirect techniques. (b) Volume acceleration method with MV. (c) NFH method with MV. (d) Far-field extraction method with MV. (e) Far-field extraction method with air guns.

Conclusions

Our journey to develop a viable modern MV option well suited for commercial application was completed with a successful field test in the North Sea. We reliably emitted signals over a desired bandwidth without creating extraneous HF noise (an undesirable characteristic of air guns). The tools we developed provide a predictable and accurate estimate of the far-field wavelet signature, which is much more straightforward than predicting air-gun bubble interaction. At our test facility, we demonstrated our ability to generate a wide variety of signal types that are useful for crosstalk removal — an important factor for high productivity using simultaneous/continuous shooting. Our MV design produced a versatile well-controlled source with excellent repeatability.

It would seem that what is old is new again. Whether or not MVs will actually become the workhorse of the future for acquiring commercial marine seismic surveys remains an open question. The benefits of this technology in terms of environmental impact, acquisition efficiency, data quality, etc. are subject to further evaluation by the industry such as the Environmental Assessment of Marine Vibroseis project conducted by the E&P Sound and Marine Life Joint Industry Programme. Although the technology is now available, its future take-up will ultimately depend on the outcomes of such studies and industry needs. **TLE**
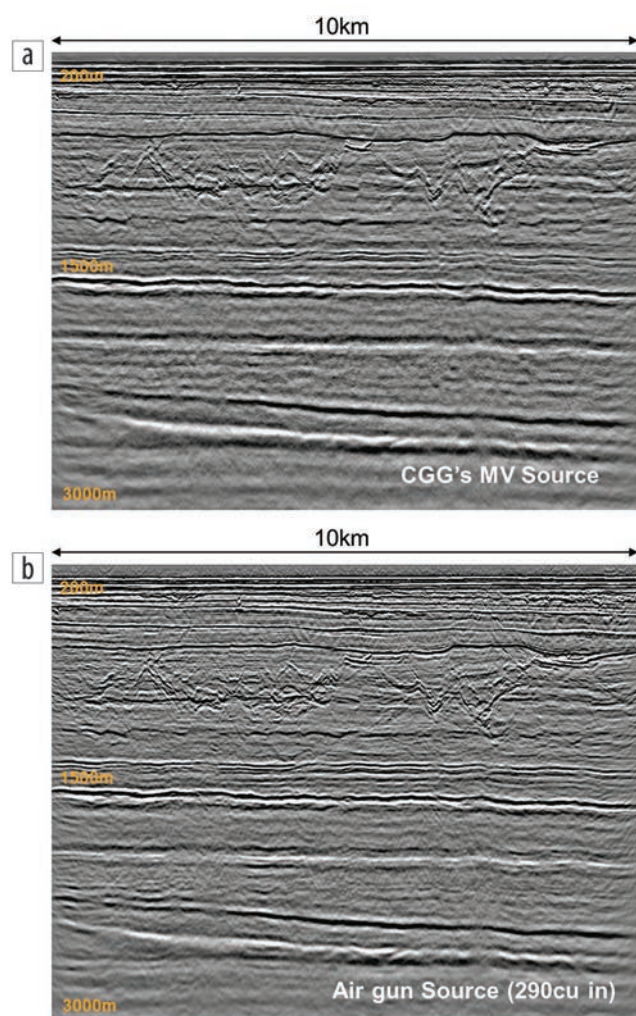
Figure 9. Comparison between two seismic sections obtained along the same 2D line acquired in the North Sea. (a) Seismic image obtained with CGG's MV source. (b) Seismic image obtained with an air-gun source of 290 in³.

Acknowledgments

Data and materials availability

Data associated with this research are confidential and cannot be released.

Corresponding author: benoit.teyssandier@free.fr

References

Baeten, G., J. Fokkema, and A. Ziolkowski, 1988, The marine vibrator source: First Break, **6**, no. 9, 285–294, https://doi.org/10.3997/1365-2397.1988016.

Bouyoucos, J. V., and D. E. Nelson, 1988, A marine digital hydraulic vibrator: Part 1 — Concepts and coding techniques: Presented at Offshore Technology Conference.

Broding, R. A., J. M. Hess, and R. E. Wanous, 1971, A high-power computer-controlled marine Vibroseis® system: IEEE Transactions on Geoscience Electronics, **9**, no. 2, 90–95, https://doi.org/10.1109/TGE.1971.271472.

Caldwell, J., and W. Dragoset, 2000, A brief overview of seismic air-gun arrays: The Leading Edge, **19**, no. 8, 898–902, https://doi.org/10.1190/1.1438744.

Dellinger, J., A. Ross, D. Meaux, A. Brenders, G. Gesoff, J. T. Etgen, and J. Naranjo, 2016, Wolfspar®, an "FWI-friendly" ultra-low-frequency marine seismic source: 86th Annual International Meeting, SEG, Expanded Abstracts, 4891–4895, https://doi.org/10.1190/segam2016-13762702.1.

Hegna, S., T. Klüver, and J. Lima, 2018, Making the transition from discrete shot records to continuous wavefields — Methodology: 80th Conference and Exhibition, EAGE, Extended Abstracts, https://doi.org/10.3997/2214-4609.201800998.

Hovem, J. M., T. V. Tronstad, H. E. Karlsen, and S. Lokkeborg, 2012, Modeling propagation of seismic airgun sounds and the effects on fish behavior: IEEE Journal of Oceanic Engineering, **37**, no. 4, 576–588, https://doi.org/10.1109/JOE.2012.2206189.

Jenkerson, M., J. Hopperstad, G. Johnson, J.-M. Mougenot, and B. Rosenbladt, 2013, Marine vibrator JIP: 75th Conference and Exhibition, EAGE, Extended Abstracts, https://doi.org/10.3997/2214-4609.20131196.

Laws, R., D. Halliday, J.-F. Hopperstad, D. Gerez, M. Supawala, A. Özbek, T. Murray, and E. Kragh, 2018, Marine vibrators: The new phase of seismic exploration: Geophysical Prospecting, **67**, no. 6, 1443–1471, https://doi.org/10.1111/1365-2478.12708.

Mougenot, J.-M., S. Griswold, M. Jenkerson, and R. Abma, 2017, Next-generation marine seismic sources: A report from the SEG 2015 postconvention workshop: The Leading Edge, **36**, no. 7, 598–603, https://doi.org/10.1190/tle36070598.1.

Rassenfoss, S., 2016, Offshore seismic feeling pressures to change: Journal of Petroleum Technology, **68**, no. 1, 32–37, https://doi.org/10.2118/0116-0032-JPT.

Robinson, C. L., 1967, How vibratory seismic work is conducted offshore: World Oil, 130–132.

Rossi, M., 1988, Acoustics and electroacoustics: Artech House Inc.

Sallas, J., 2010, How do hydraulic vibrators work? A look inside the black box: Geophysical Prospecting, **58**, no. 1, 3–17, https://doi.org/10.1111/j.1365-2478.2009.00837.x.

Sallas, J., 2014, Process for separating data recorded during a continuous data acquisition seismic survey: U.S. Patent 8,724,428.

Sherman, C. H., and J. L. Butler, 2008, Transducers and arrays for underwater sound: Springer.

Tenghamn, R., 2009, Driving means for acoustic marine vibrator: U.S. Patent 7,551,518.